9 PAPER 4

Comparison of geomorphological field- and 2D InSAR mapping of the periglacial landscape at Nordnesfjellet, Northern Norway

*Eckerstorfer, M.[1]., Eriksen, H.Ø.[1], Rouyet, L.[1], Christiansen, H.H.[2], Lauknes, T.R.[1], Blikra, L.H.[3,4].

[1]Norut, P.O. Box 6434 Tromsø Science Park, 9294 Tromsø, Norway
[2]Arctic Geology Department, The University Centre in Svalbard, UNIS, P.O. Box 156, 9171 Longyearbyen, Norway
[3]Norwegian Water Resources and Energy Directorate, NVE, P.O. Box 5091 Majorstua, 0301 Oslo, Norway
[4]Geology Department, The Arctic University of Norway Tromsø, UiT, P.O. Box 6050 Langnes, 9037 Tromsø, Norway

**Corresponding author:* Norut, P.O. Box 6434 Tromsø Science Park, 9294 Tromsø, Norway. E-mail address: markus.eckerstorfer@norut.no (M. Eckerstorfer).

Abstract

The ability to continuously monitor the dynamic response of periglacial landforms in a climate change context is of increasing scientific interest. Satellite radar interferometry provides information on surface displacement that can be related to periglacial processes. Here we present a comparison of 2D surface displacement rates and geomorphological mapping at periglacial landform-scale from the mountain Nordnesfjellet in Northern Norway. 2D InSAR results stem from a 2009-2014 TerraSAR-X dataset from ascending and descending orbits, decomposed into horizontal displacement vectors along a W-E plane, vertical displacement vectors and combined displacement velocity. Geomorphological mapping was carried out on aerial imagery and validated in the field. Detailed landform and sediment type mapping revealed an altitudinal distribution with high-elevation, weathered bedrock blockfields, surrounded primarily by slightly, to non-vegetated solifluction landforms. Below, an active rockslide and associated rockfall deposits are located on the steep east-facing side of the study area, whereas glacial tills dominate on the gentler western side. We could show that 2D InSAR correctly depicts displacement rates that can be associated with typical deformation patterns for flat-lying or inclined

landforms, within and below the regional permafrost limit, for both wet and dry areas. Using substantial time series of both field and InSAR observations, future monitoring of periglacial landscapes in a changing climate becomes feasible.

Keywords: 2D InSAR, periglacial landforms, permafrost, geomorphological mapping, remote sensing

1. Introduction

Mountainous landscapes in periglacial environments are highly sensitive to climate change (e.g. Etzelmüller, 2013). Haeberli (2013) identified two slope stability problems in mountains underlain by permafrost: accelerated creep of perennially frozen talus/debris with high ice contents on moderately steep slopes and decreasing stability of steep, frozen rock walls. In both cases, high permafrost temperatures and / or the shift of the altitudinal limit of permafrost occurrence are critical. Periglacial mountain landscapes exhibit a variety of landforms under changing topographical and environmental conditions. Moreover, different periglacial landforms contain various amounts of ground ice. A change in environmental factors and a thawing or potential degradation of particularly ice-rich sediments can lead to substantial landscape change, with impacts on infrastructure from a geohazard perspective, as well as on ecosystems (Brown et al., 2008).

The Nordnesfjellet mountain in Northern Norway is located in the sporadic permafrost zone (Gisnås et al., 2016) with an altitudinal permafrost limit of around 600 m a.s.l. (Blikra & Christiansen, 2014). It is surrounded by a high-relief fjord landscape were most hillsides are covered by colluvium from rockfall and to some degree snow avalanche activity. The higher plateaus have wide extensive weathered materials, blockfields and glacial till with periglacial activity (Tolgensbakk and Sollid, 1988). Little is known about the detailed landform variability and their level of activity in the periglacial landscape. Geomorphological studies of periglacial landscapes traditionally rely on detailed field mapping and process monitoring of the individual landform activity, including their deformation rates (Harris et al., 2009). Such measurements provide a better process understanding and are usually based on point observational data, which can be extrapolated to landscape-scale, using for example geostatistical modeling (e.g. Hjort and Luoto, 2013; Hjort et al., 2014). To enable the analysis of large, remote areas, remote sensing data are required. Interferometric Synthetic Aperture Radar (InSAR) is such a new innovative method that can provide landscape-scale surface deformation. Kenyi and Kaufmann (2003) and Strozzi et al. (2004) were among the first to use InSAR for permafrost related ground displacement measurements over large areas. Since then, InSAR was used to measure permafrost related ground displacement at Herschel Island, Canada (Short et al., 2011), the Tibetan Plateau, China (Chen et al., 2013) and Northern Alaska Liu et al. (2010) and Liu et al. (2012). The InSAR datasets were mostly used as stand-alone datasets for the detection and inventory of moving objects, the evolution of permafrost degradation and associated ground surface sinking. However, Shur et al. (2005) used the acquired displacement rates to drive a model of active layer development, showing that thaw settlement was due to melting of the transient layer.

In this study, we use satellite-borne 2D InSAR to quantify periglacial landform specific displacement rates. We achieve this by comparing mapped periglacial landforms at the Nordnesfjellet mountain in Northern Norway with a multi-geometry TerraSAR-X dataset from 2009-2014. We discuss possibilities and limitations in using InSAR as a tool for geomorphological mapping and monitoring of periglacial landform dynamics and the state of the mountain geomorphology at Nordnesfjellet.

2. Study area

The roughly 8-km^2 large study area is centered over the Jettan rockslide at Nordnesfjellet mountain in Northern Norway (Figure **1**a). From the study area's highest point at 900 m a.s.l., the entire west-facing hillside, where the rockslide is located, is included in the analysis. To the east, the study area extends down to an elevation of about 500 m a.s.l. in its northeastern corner (Figure **1**a). The delineation of the study area is the result of the coverage of available aerial images, digital terrain models, and long-term SAR datasets. Mean annual air temperature is slightly above freezing at 700 m a.s.l., with annual amounts of precipitation at around 300 mm (MET, 2017). The regional climatic tree line is presently at 250 m a.s.l., characterized largely by birch trees. The bedrock in the area consists of well-foliated gneisses and intercalated marble and schists overlain by Quaternary sediments with Holocene periglacial reworking by diverse slope and weathering processes (Braathen et al., 2004).

3. Methods

3.1 Geomorphological mapping

Geomorphological mapping was based on photogrammetric aerial image interpretation and field verification. We used the 'Stereo Analyst' toolset of ArcGIS 10 on a 3D monitor to do the geomorphological mapping of the study area. Aerial image stereo pairs (0.4 m spatial resolution) and a DEM (10 m spatial resolution) were acquired from the Norwegian Mapping Authority.

First, we determined the most prominent periglacial landforms and slope processes and mapped them at a scale of 1:10 000, focusing on landforms and sediments. We then validated the photogrammetric interpretations in the field in June 2013, clarifying uncertainties in the digital interpretation. Nomenclature and landform codes are according to the code list used by the Geological Survey of Norway (NGU).

3.2 InSAR data and processing

We produced InSAR data from snow free scenes (roughly June–October) in the period 2009–2014 using TerraSAR-X Stripmap Mode radar satellite data. For each geometry (ascending/descending orbits), approximately 160 combinations of SAR scenes (or interferograms) were selected. To minimize temporal decorrelation and to be able to capture fast moving objects, we used a maximum interval between scenes (or temporal baseline) of 55 days and removed low coherence interferograms from early spring and late autumn because of a snow-covered surface. The mean annual velocity of each pixel for the ascending and descending datasets was computed by weighted averaging (stacking) of all interferograms from the entire period (Price and Sandwell, 1998). By doing so, displacement measurements from the snow-free seasons were used to retrieve mean annual velocities, assuming the same velocity for the snow-free and snow-covered periods of each year.

The InSAR ascending and descending datasets were then calibrated relative to a point of known velocity. Here we used a 3 x 3 pixel area covering a GNSS station outside the Jettan rockslide. The calibrated InSAR datasets were compared to the GNSS station data, using the mean difference between both datasets to recalibrate the InSAR dataset once more. After the calibration procedure, the resulting magnitude of displacement was consistent with the data from 6 of the GNSS network's stations covered by InSAR data, thus considered as reliable for interpretation of displacement patterns (Eriksen et al., 2017).

3.3 Decomposition into 2D InSAR

The InSAR method is only sensitive to displacement along the radar line-of-sight (LOS). At Nordnesfjellet, the LOS is 78/45 and 283/53 (azimuth/dip), respectively for the ascending and the descending orbit geometries. The radar is not capable of detecting any displacement orthogonal to the LOS-vector. Relating InSAR displacement maps to surface displacements can be difficult, especially when surface displacements are close to the blind plane, defined by the two LOS vectors. The 2D InSAR method combines ascending and descending InSAR datasets into a 2D displacement vector surface, increasing the interpretability (Figure **1**c). Thus, vectors in the east-west plane can be calculated and decomposed into horizontal and vertical components (Eriksen et al., 2017). Nevertheless, since the sensor is side looking and orbits are almost north - south, 2D InSAR is not capable of detecting northward or southward deformation. In order to minimize errors due to underestimation in the north-south direction, we used a relatively conservative mask, selecting only pixels within +/- 22.5° aspect in the east and west directions (Figure **1**d). As a result, 33.6 % of the study area was covered by 2D InSAR results, masking out northerly and southerly aspects predominantly found on the high-lying plateaus. There is moreover almost no coverage on the lower west-facing slopes where forested areas decorrelate the InSAR signal. The final geocoded InSAR results are mean velocity maps over the period 2009–2014 expressed in mm/yr with 10 m pixel spacing. All processing steps were performed with the Norut GSAR software (Larsen et al., 2005).

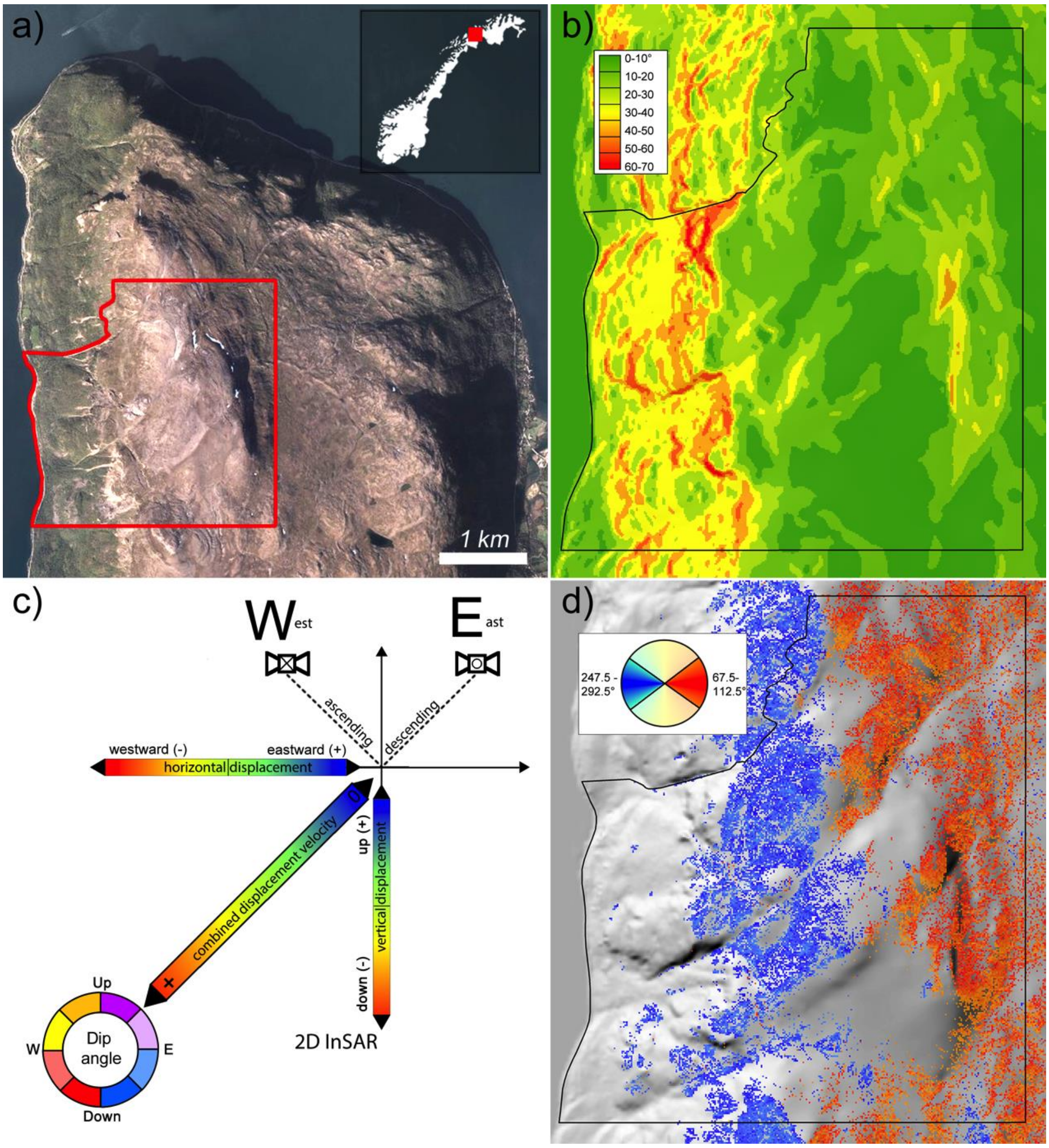

Figure 1: a) Aerial image showing the Nordnesfjellet mountain peninsula in Northern Norway with the study area marked in red. b) Slope angle map with 10° increments. c) West-east cross-section with 2D InSAR horizontal, vertical and combined displacement velocity from decomposition of InSAR data from ascending and descending satellite orbit observed along the instruments line-of-sight (LOS) vectors. Color scales show displacement rates and aspect of displacement in maps and figures. d) Study area map showing selected areas in aspects 67.5–112.5° and 247.5–292.5°.

4. Results

4.1 Periglacial landform variability at Nordnesfjellet

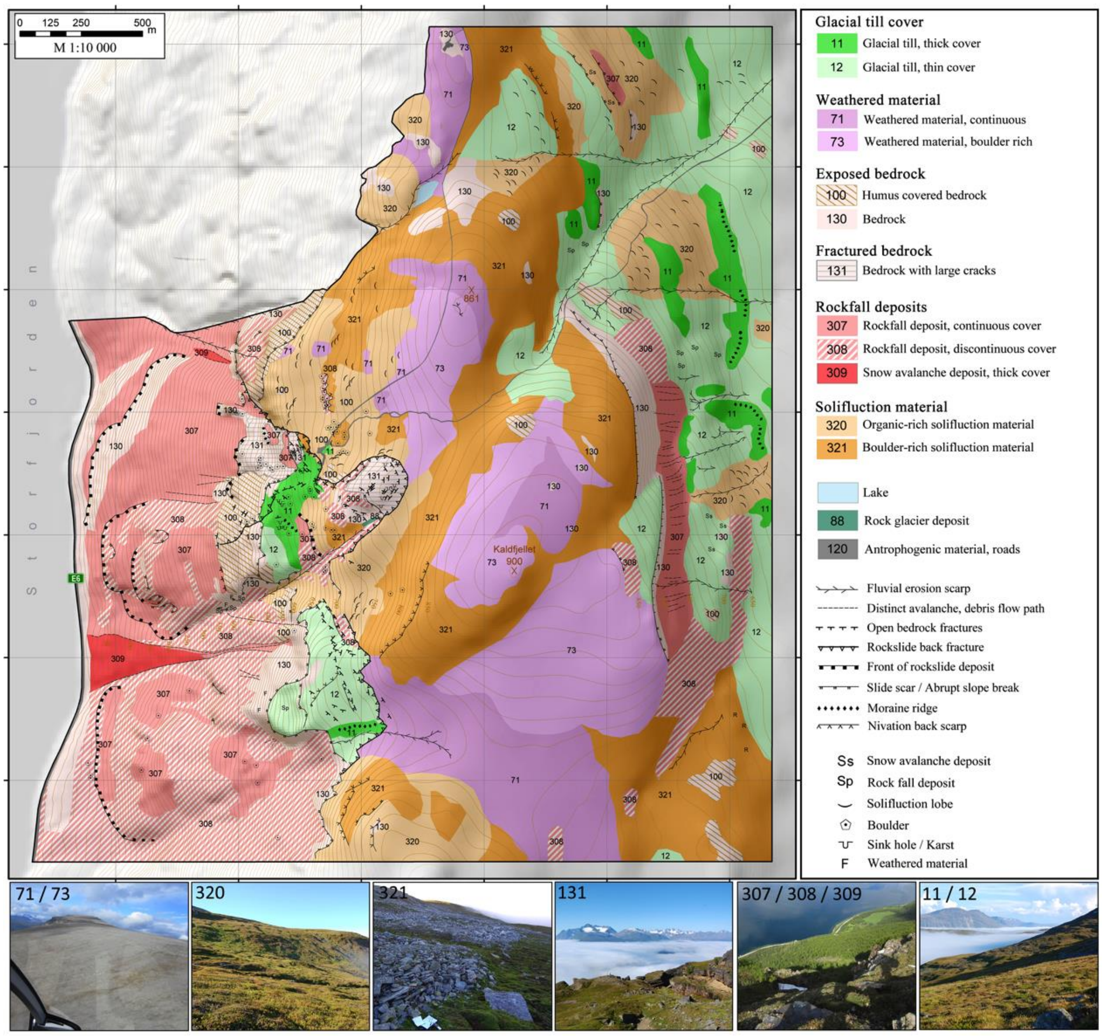

Figure 2: Geomorphological map in scale 1:10000 of the Nordnesfjellet study area. Both periglacial sediments and landforms are shown, colored and coded as described in the legend. For further analysis we classified the identified periglacial landforms into six geomorphological classes. Pictures (coded accordingly) show various landforms mapped.

The overall distribution of periglacial landforms in the study area is largely governed by aspect, slope angle, and elevation as topographic parameters, and landscape-scale permafrost occurrence (Figure **2**). The highest, flat to low-inclined plateau areas located above the regional permafrost limit (ca. 600 m a.s.l.) are vegetation free, relatively dry, and covered by continuous (dark purple, code 71) and boulder rich (light purple, code 73) weathered material. These areas covered in weathered material are on average 7° steep, located at elevations above 655 m a.s.l. (Figure **3**). Here, daily and seasonal heave and thaw settlement, and associated periglacial sorting take place.

The high-lying plateaus are surrounded by areas that are fully vegetated and covered in organic-rich solifluction material (light orange, code 320), as well as sparsely vegetated, boulder rich solifluction material (dark orange, code 321) (Figure **2**). These areas covered in solifluction material are found in an elevation band between 480–900 m a.s.l. at the boarder of regional permafrost, with slope angles averaging 15°. Outliers can be found towards steeper terrain, especially for the boulder-rich solifluction lobes and sheets (Figure **3**).

Decreasing further in elevation, the dominantly west and east-facing hillside of the study area are significantly different in periglacial landform occurrence, slope angle and elevations covered. The west-facing hillside is dominated by the active Jettan rockslide (fractured bedrock, light purple, code 131) and rockfall deposits (light red, codes 307 and 308) (Figure **2**). Former, referred to as areas with fractured bedrock, cover areas from 270–805 m a.s.l. with slope angles of up to 70° and a median of 39°. The associated rockfall deposit covered slopes extending to sea level, with a median slope angle of 34°. These areas appear to be active, evident from loose rocks, perched boulders, and broken trees.

The east-facing hillside on the other hand is covered by Younger Dryas moraines (thick glacial till cover, code 11 in dark green) and thinly glacial till covered areas in between (light green, code 12) (Figure **2**). These glacial till covered areas are characterized by low-inclined terrain (average of 13°) in elevations between 490–850 m a.s.l. (Figure **3**).

In terms of areal coverage, solifluction material covers 31.5 % of the study area, followed by areas covered in rockfall deposits with 23.8 % and weathered material-covered areas with 18.7 %. Exposed bedrock areas cover 7.1 % while the fractured bedrock areas of the Jettan rockslide cover 2.7 % of the total study area (**Figure 4**).

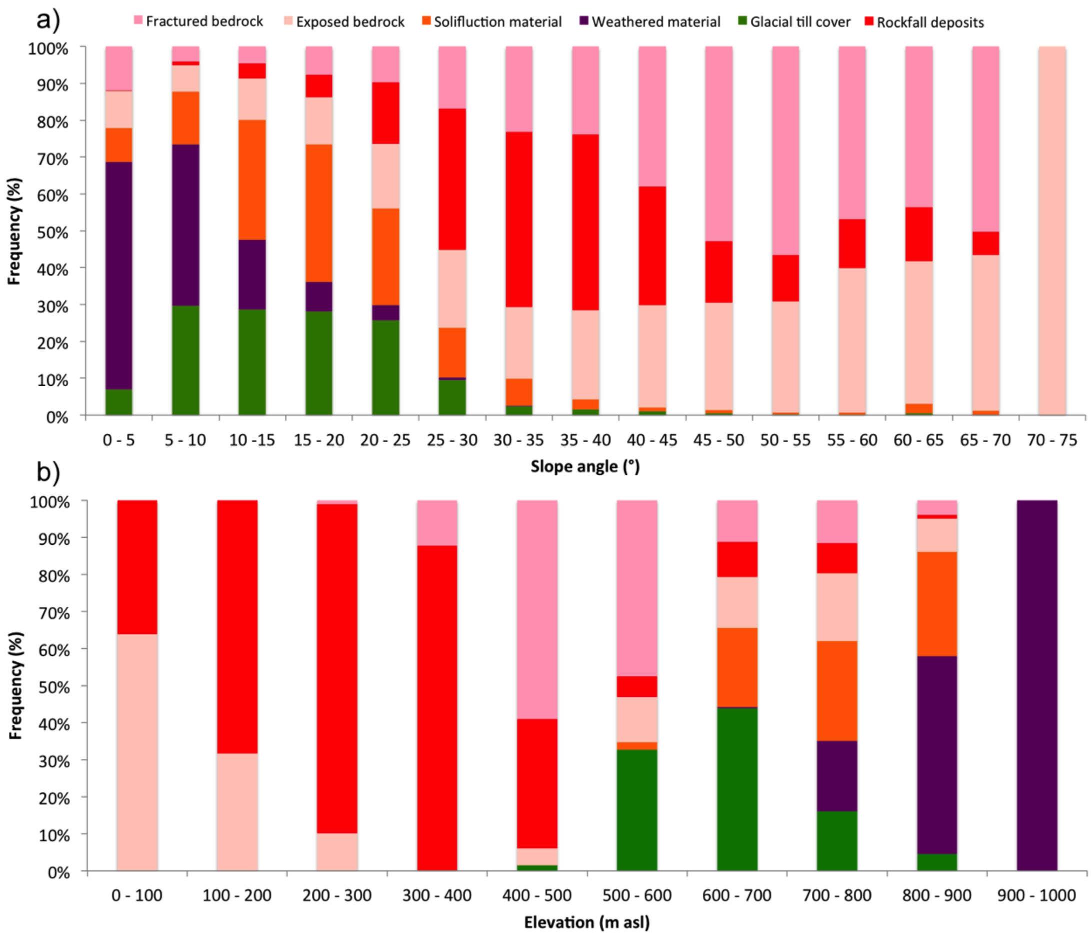

Figure 3: Histograms of pixel frequency per a) slope angles and b) elevations covered by the six geomorphological classes.

4.2 2D InSAR landscape-scale combined displacement velocities

The six aggregated geomorphological classes are different in spatial extent as we masked out aspects diverging more than 22.5 degrees from east and west. Moreover, the distribution of 2D InSAR pixels per geomorphological classes is also highly variable (Figure **4**). We therefore randomly selected 1000 pixels per class for further 2D InSAR analysis and comparison with the geomorphological mapping.

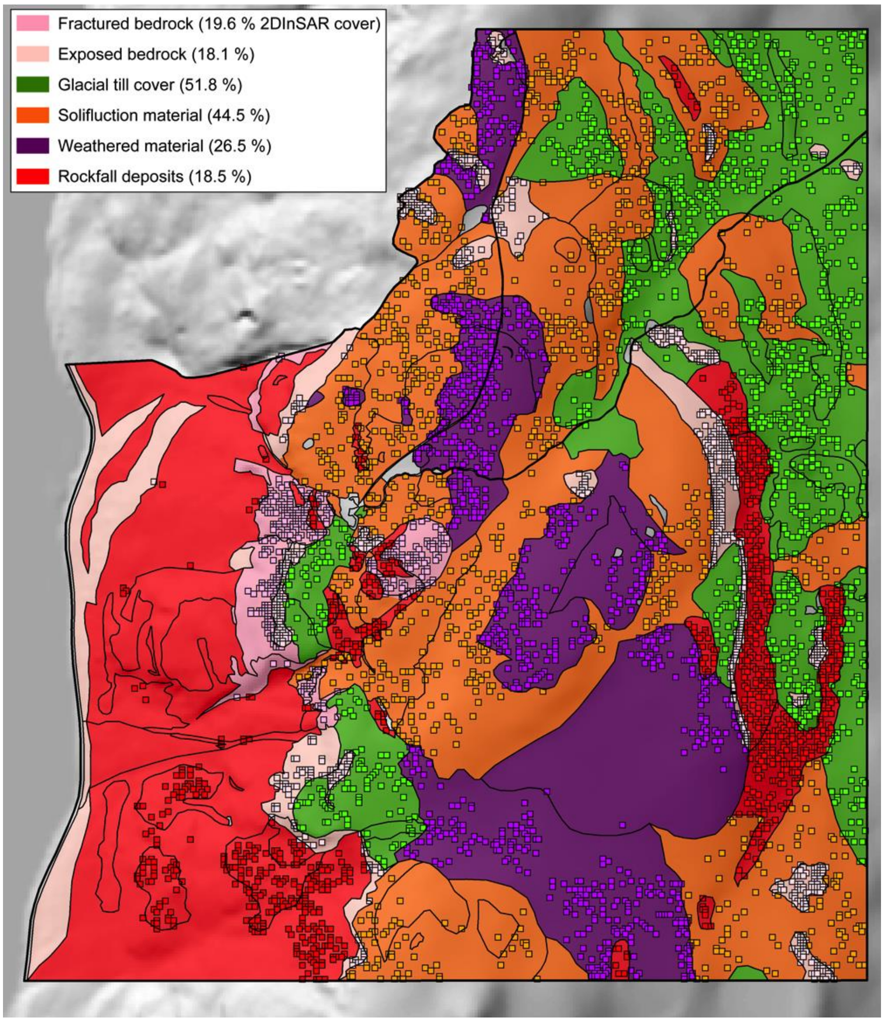

Figure 4: Map of the study area showing all six geomorphological classes with the percentage of pixels covered by 2D InSAR data. As a result of differential 2D InSAR data coverage, 1000 random pixels per class (visualized by colored squares) were chosen for further analysis.

The study area experienced an average combined displacement velocity of 10–15 mm/yr with downward dip angles, indicating an overall settlement of the landscape (Figure **5**). High horizontal westward components characterized the active Jettan rockslide. The displacements were mainly downward but areas with upward trends were also detected. These heterogeneous displacement patterns may indicate a complex fault geometry at depth (Eriksen et al., 2017). The rockslide area exhibited furthermore the highest combined displacement velocities together with areas that were mapped as rockfall deposits and solifluction material on the east-facing slopes of the study area (Figure **2**, Figure **5**). Especially solifluction landforms beneath steep slopes experienced a steady moisture source, which can result in high solifluction rates. Lower than average combined displacement velocities were visible on high-elevation west-facing slopes covered by weathered material and solifluction material (Figure **2**, Figure **5**). These areas were low-inclined to flat and likely dry, thus only minor frost heave and settlement could occur.

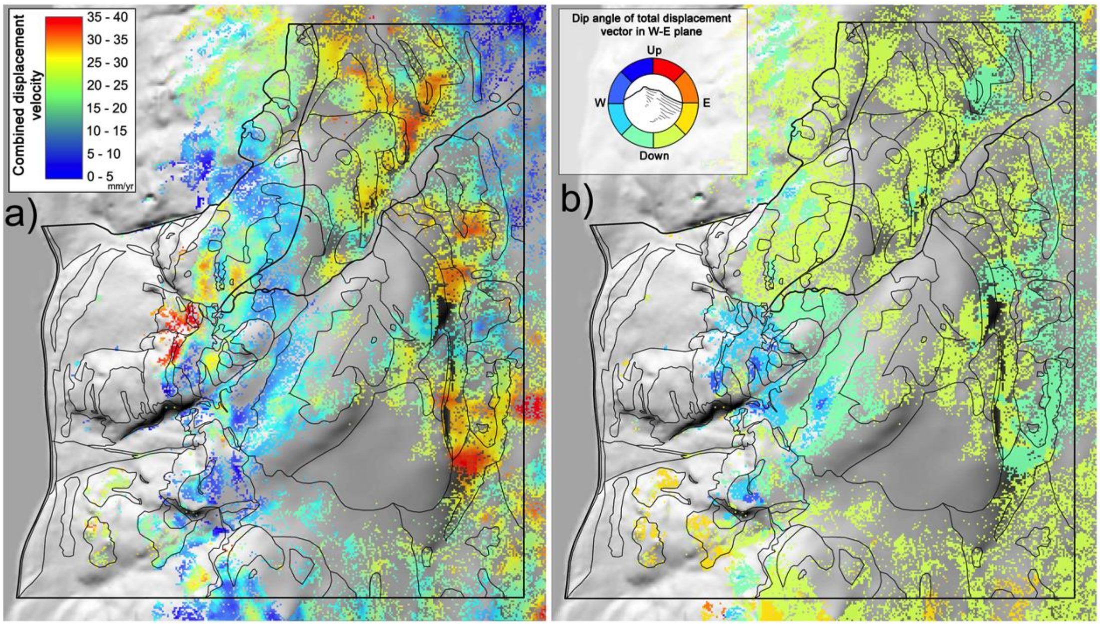

Figure 5: a) Map of 2D InSAR combined displacement velocities. Rates are in mm/yr (2009–2014). b) Dip angle of 2D displacement vectors in west-east plane. The thick black lines outline the different periglacial landforms, mapped in Figure 2.

4.3 2D InSAR landform-scale displacement velocities

High-lying areas covered in glacial till, weathered material and solifluction material, as well as exposed bedrock areas experienced the lowest average combined displacement velocities ranging between 0–30 mm/yr (Figure **6**). The higher ranges in combined displacement velocities were mainly measured from rockfall deposits and fractured bedrock areas, which are driven by gravitational processes.

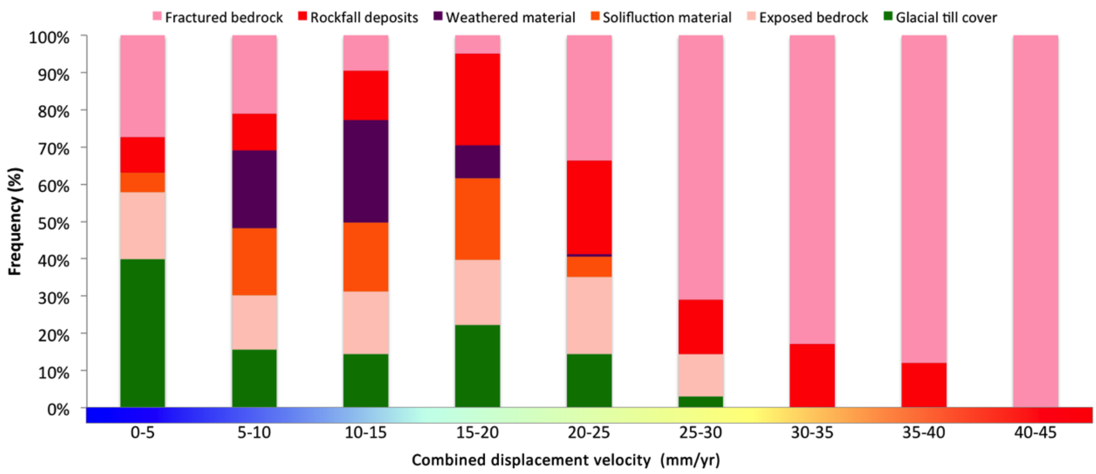

Figure 6: Histograms of pixel frequency per combined displacement velocity range of 5 mm increments for the six geomorphological classes.

Combined displacement velocities can be divided into horizontal and vertical displacement vectors (Figure **1**c), which we present for each of the six geomorphological classes in Figure **7**. The total net surface lowering visible also in Figure **5** is shown in a dominating vertical downward displacement in all classes. Weathered material-covered areas experienced no upward movement, while all other classes experienced areas with minor uplift as well. Skewness of the horizontal component towards west or east was mostly a function of the occurrence of a geomorphological class in the study area. This is evident from glacial till covered areas mostly occurring on the east-facing side, while fractured bedrock areas were mostly found on the west-facing side of the study area (Figure **2**). Areas covered in weathered material had the lowest inter-class standard deviation for horizontal and vertical displacement with 2.4 and 3 mm/yr respectively, as this class was rather homogeneously distributed in elevation and slope angle. Rockfall deposits and fractured bedrock areas were found at wider elevation bands and slope angles, experiencing thus horizontal and vertical displacement rates with large standard deviations of up to 9 mm/yr (Figure **7**).

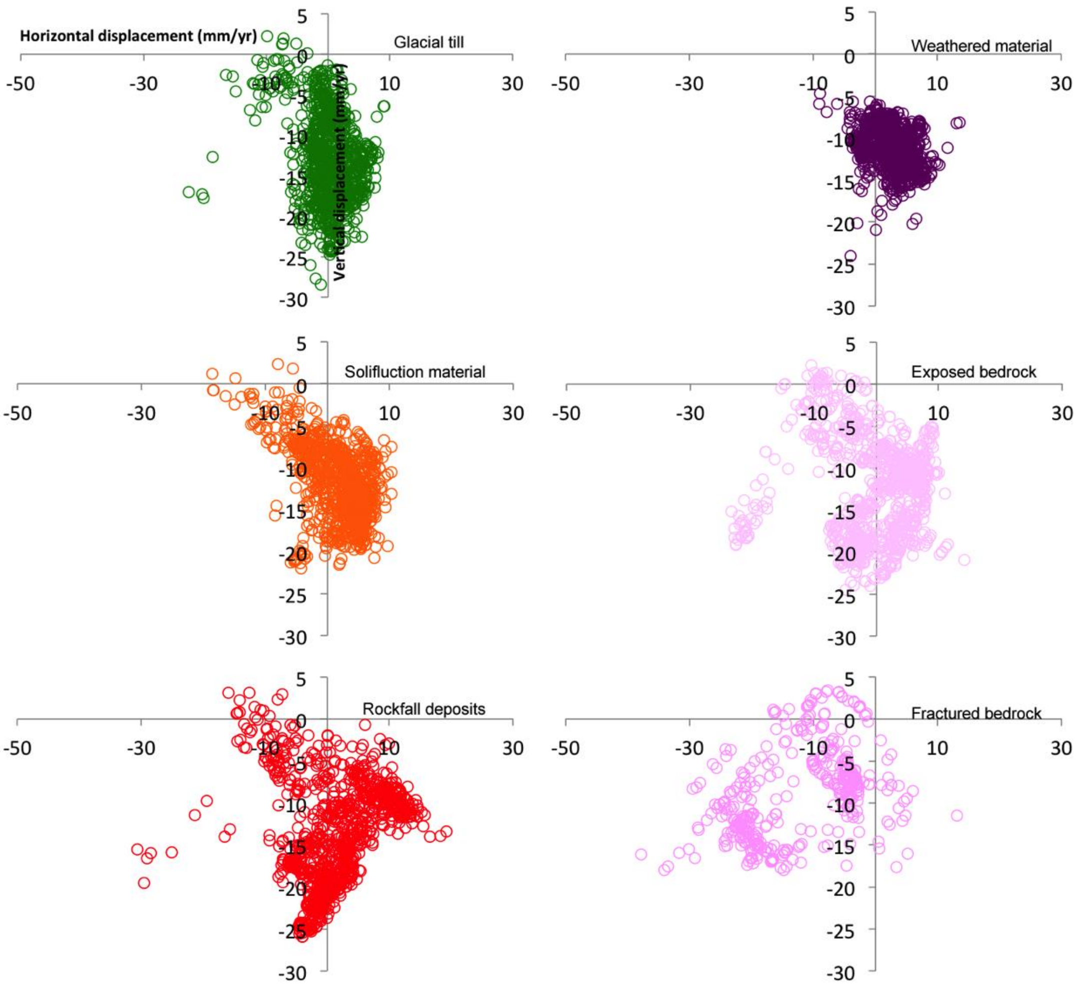

Figure 7: Scatterplots showing horizontal and vertical displacement rates of 1000 randomly chosen pixels within each of the six geomorphological classes.

5. Discussion

5.1 Quantitative geomorphological interpretation of 2D InSAR results

Periglacial landforms are influenced by topographical and meteorological factors at different scales. Topographical factors including slope angle and elevation act on a landscape-scale, largely controlling the occurrence and activity level of periglacial landforms. The study area can be roughly divided into two parts: Flat areas to gentle slopes at elevations above the regional permafrost limit, and steep slopes with fast downslope displacement rates at lower elevations. Comparing each geomorphological class in terms of their slope angle and elevation distribution, they can be divided into flat to low-inclined high elevation landforms (glacial till, weathered material and solifluction material) and steep, low elevation landforms (exposed bedrock, rockfall deposits and fractured bedrock) (Figure **8**). Areas covered in glacial till, weathered material and solifluction material exhibited median slope angles between 7–15°, while areas covered in rockfall deposits and different bedrock areas had median slope angles between 30–40°. The median elevation for the latter group was 554 m, roughly 200 m lower than for the high elevation landforms and thus presumably also below the regional permafrost limit. Considering the interquartile range of each geomorphological class, the high elevation group had a three times smaller interquartile range compared to the low elevation group. The interquartile range in slope angles was two times smaller for the high elevation group than for the low elevation group.

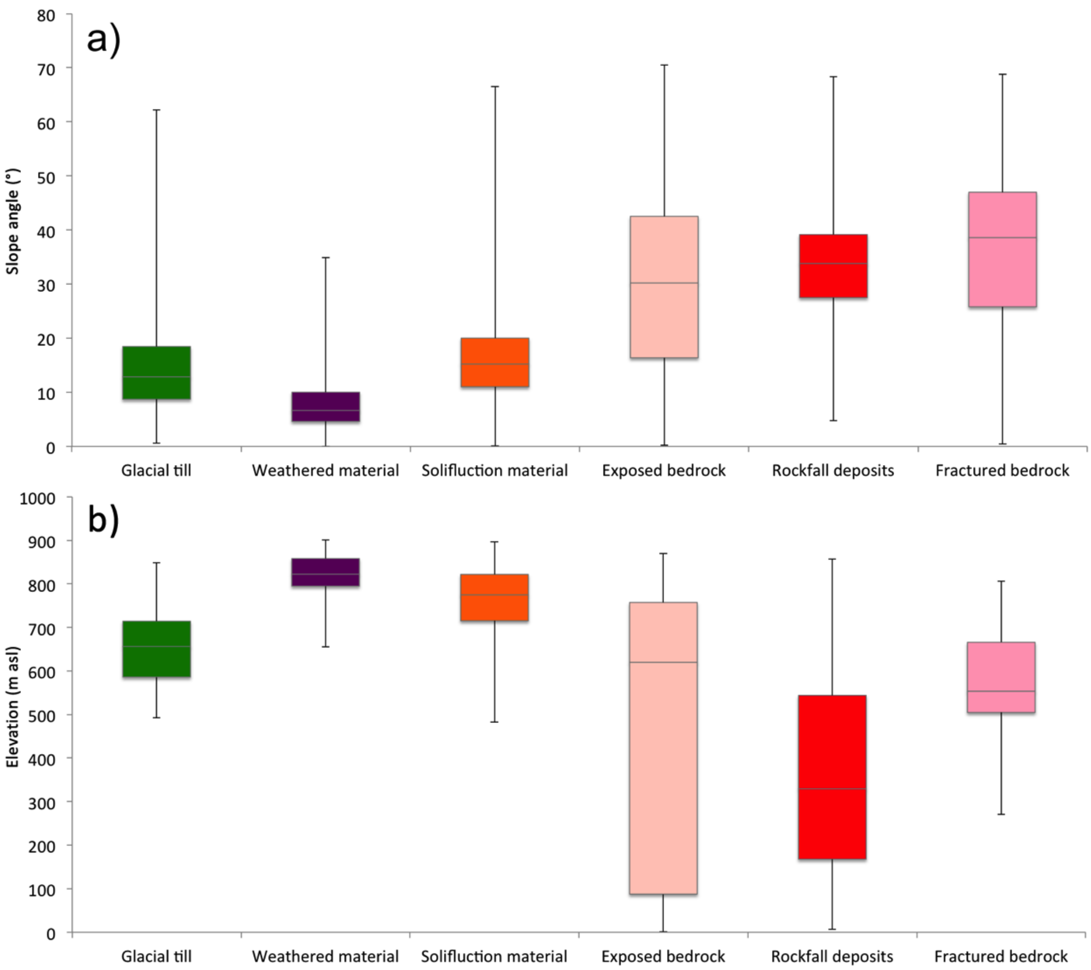

Figure 8: Boxplots showing median, interquartile range and min / max outliers of a) slope angle and b) elevation for all six geomorphological classes.

The presence of permafrost, a prerequisite for active periglacial landscapes can only indirectly be observed using remote sensing (e.g. Kääb et al., 2005). Using InSAR, the state of activity and process speeds both within periglacial landforms and between them can be measured and quantified. From Figure **5** it is evident that surface deformation took place, resulting in an overall net lowering of the surface. However, it became also evident from Figure **6** and Figure **7** that 2D InSAR displacement rates were not significantly different between geomorphological classes. This is especially true for the class-specific median combined displacement velocities, which ranged between 11.8 mm/yr for areas covered in weathered material and 15.9 mm/yr for rockfall deposits (Figure **9**). Only maximum outliers and the interquartile range of each geomorphological class held differentiating information.

Maximum outliers of combined displacement velocity were presented in Figure **3**. The interquartile range is a measure of entropy within the geomorphological classes, hinting towards larger variability in combined displacement velocities in the three low-elevation classes (Figure **8**). The other three high-lying classes showed low standard deviations in combined displacement velocities in line with their more homogenous distribution in elevation and slope angle (Figure **8**).

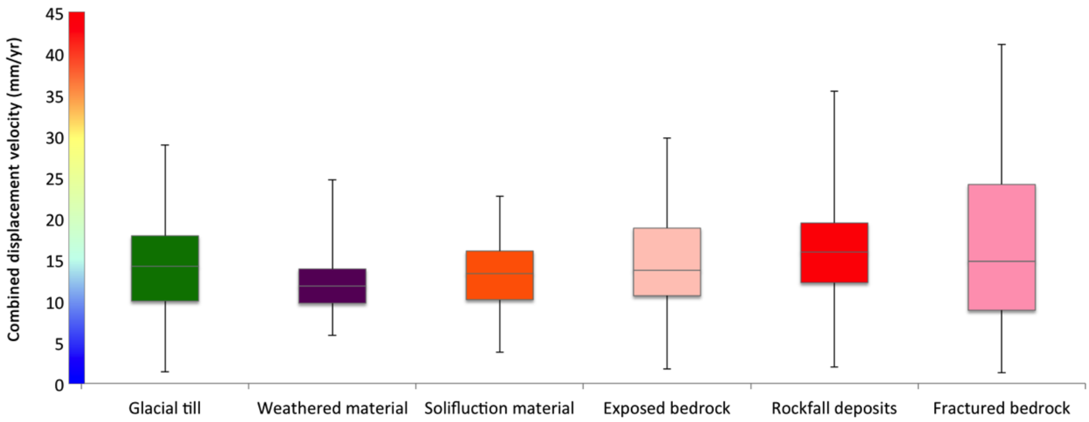

Figure 9: Boxplots showing median, interquartile range and min / max outliers of combined displacement velocities for all six geomorphological classes.

5.2 Qualitative geomorphological interpretation of 2D InSAR results

Mountainous areas in polar regions carry landform evidence from intense glaciations such as rock walls and glacial till deposits. Morphodynamic processes in the mountains are comparable to other landscapes. However, intensity and rates are higher because of the steep terrain providing energy for erosion and sediment transport. Furthermore, denudation is also high because of low temperatures and increases precipitation (Barsch and Caine, 1982). Caine (1974) identified different controlling factors, responses and levels of activity in the periglacial mountain sediment cascade, of which the coarse debris system and the fine clastic sediment system exist at Nordnesfjellet:

The coarse debris system is effective in debris transport and incorporates rockfall, snow avalanche activity and slope failures such as rockslides. The geomorphological work of snow avalanches is of minor importance at Nordnesfjellet, we have thus classified the entire colluvium as rockfall deposits. These deposits need a large source area of rock fall to develop, thus they are mostly found on the lower parts of the steep west-facing mountain side beneath the active Jettan rockslide. 2D InSAR correctly identified high combined displacement velocity with a downslope dip angle that characterize the rockfall deposits, and fractured bedrock areas which are all part of the Jettan rockslide. Here, displacement patterns and rates showed a larger variability, which are explained in detailed by Eriksen et al. (2017). Many studies have shown the great variability of talus accumulation and movement in space and time (summarized by Barsch and Caine, 1984) and the variability of the displacement rates might be a proof of this.

The fine sediment system includes besides bedrock weathering also the mass wasting processes of alpine slopes. This system mostly responds to the freezing and thawing of the ground, the distribution of snow, and the amount of precipitation. Thus, in wetter sites, mass wasting by frost creep and solifluction are greater. Areas covered in weathered material are commonly referred to as blockfields (Ballantyne, 1998). Blockfields are high elevation, dry areas, mainly subject to annual frost heave and thaw settlement, with the rate of vertical displacement being largely influenced by active layer thickness. At Nordnesfjellet, shallow borehole data from 908 m a.s.l.. indicate a mean annual ground temperature just below 0°C, and an active layer thickness beyond 2.5 m (Harris et al., 2009). 2D InSAR data showed overall consistent minor downward displacement of the blockfield areas.

The solifluction landforms occurring below the blockfields on mostly low-inclined wet surfaces typically are the most widespread landforms in periglacial landscapes (Matsuoka, 2001). The solifluction sheets and lobes showed 2D InSAR displacement rates typical for solifluction in a discontinuous permafrost zone. 2D InSAR further correctly indicated a combination of vertical and horizontal components that is inherent for solifluction, depicted by westward and eastward displacement rates, according to the solifluction landforms exposure to aspect. Solifluction landforms stretch below the discontinuous permafrost limit, also observed by Hjort et al. (2014) in the Nordnes area. Presumably primarily one-sided, diurnal frost and needle ice creep account for these low-lying solifluction features (Harris et al., 2008; Matsuoka, 2001). Annual surface velocities, according to a review by Matsuoka (2001) in areas with frequent diurnal freeze-thaw cycles, as well as a warm, discontinuous permafrost zone are in the range of 10–15 cm. This is in accordance with the 2D InSAR measurements from the study area.

The location of areas covered in glacial till is topographically controlled by the upper limit of the last glaciation during the Younger Dryas (Kverndal and Sollid, 1993) causing deposition of a thin glacial till cover, as well as clearly visible moraines. These landforms showed only minor deformation rates in the 2D InSAR maps, typical for fine-grained, dry surfaces that lie below the regional permafrost limit.

5.3 Potential and limitations using 2D InSAR

Combining InSAR surface displacements from ascending and descending geometries provides a powerful tool to study surface displacement patterns at periglacial landscape-scale. We can explain the landform-scale displacement patterns and rates with our geomorphological process knowledge. However, we fall short in classifying the periglacial landscape into geomorphological classes using the 2D InSAR dataset. This is because of displacement rates overlapping significantly within and between classes, which makes the identification of threshold values impossible. Moreover, topographical and meteorological factors need to be considered as well when analyzing the distribution of periglacial landforms. Finally, the classification of geomorphological classes is based on aerial image interpretation, which is subject to certain bias and uncertainty in drawing the boarders between each class.

There are certainly limiting factors in using InSAR as a study tool for periglacial landscape activity, which are intrinsic to the method. As previously explained, the polar orbits of SAR satellites reduce sensitivity for detecting northward/southward displacements. In addition, the sensor’s wavelength and the temporal baseline of the interferograms control the range of velocities than can be measured. By selecting interferograms only from the snow free season, we expect the 2D InSAR data to contain a larger component from thaw than from freeze. Furthermore, mean annual vertical displacements are likely overestimated and can thus induce too steep dip angles. These effects are likely enhanced in the upper regions of the study area, which are underlain by permafrost.

From this study, it appears thus that exploitation of remote sensed deformation measurements for a quantitative classification of geomorphological processes at landscape-scale has a potential, but cannot be used as a standalone method. One possible way to utilize the 2D InSAR displacement rates would be to use them together with other environmental variables as a complementary input layer into statistically-based geomorphological distribution models (e.g. Etzelmueller et al., 2001; Hjort and Luoto, 2013).

6. Conclusion

From the comparison of a 2D InSAR dataset from TerraSAR-X data (2009–2014) with geomorphological mapping of the periglacial landscape of Nordnesfjellet mountain in Northern Norway, it is evident that the landscape is highly active. 2D InSAR depicts various displacement patterns and rates of six geomorphological classes that belong to either the coarse or the fine debris system of the sediment cascade of this cold mountain environment. High surface displacement rates belong to steep low-elevation terrain covered in rock fall colluvium and fractured bedrock associated with the Jettan rockslide. Lower surface displacement rates belong to low-inclined, high elevation permafrost areas covered in weathered material, undergoing solifluction. However, landform-specific displacement rates could not be clearly depicted, which suggests that 2D InSAR results has a limited value as a standalone dataset for large-scale geomorphological mapping of remote areas. Together with topographical and environmental factors, 2D InSAR results might be treated as an additional data layer for geostatistical modeling of a landscape. With the improved availability of SAR data, such methods can then be applied to large and remote periglacial mountain areas worldwide.

Acknowledgements

We would like to acknowledge both Lena Rubensdotter and Viola Renata from the Geological Survey of Norway NGU), assisting with the aerial image 3D mounting, geomorphological mapping, and interpretation. The hard-working people of NVE Kåfjord are acknowledged for valuable fieldwork assistance and logistics. The

TerraSAR-X data has been provided by the German Aerospace Center (DLR) under the TSX-AO project contract #GEO0565. This work was partly financed by the PermaSAR project, Norwegian Research Council (Project Nr: 212022/F50) and by the PermaSAT2 project, European Space Agency Prodex (Project Nr. C4000119115). Comments and suggestions for improvement from two reviewers are highly acknowledged.

References

Ballantyne, C.K., 1998. Age and significance of mountain-top detritus. Permafrost and Periglacial Processes, 9(4): 327-345

Barsch, D. and Caine, N., 1982. The nature of mountain geomorphology, Mountain Research and Development. Proceedings of a workshop of the Arbeitsgemeinschaft für Vergleichende Hochgebirgsforschung. International Mountain Society, Munich, Germany, pp. 287-298.

Braathen, A., Blikra, L.H., Berg, S.S. and Karlsen, F., 2004. Rock-slope failures in Norway; type, geometry, deformation mechanisms and stability. Norwegian Journal of Geology, 84: 67-88

Brown, J., Smith, S.L., Romanovsky, V., Christiansen, H.H., Clow, G. and Nelson, F.E., 2008. Global terrestrial network for permafrost. , Food and Agriculture Organization of the United Nations (UN FAO), Rome, Italy.

Caine, N., 1974. The geomorphic processes of the alpine environment. In: J.D. Ives and R.G. Barry (Editors), Arctic and Alpine Environments. Methuen, London, pp. 721-748.

Chen, F., Lin, H., Hong, T. and Wang, G., 2013. Surface deformation detected by ALOS PALSAR small baseline SAR interferometry over permafrost environment of Beiluhe section, Tibet Plateau, China. Remote Sensing of Environment, 138: 10-18.http://dx.doi.org/10.1016/j.rse.2013.07.006

Eriksen, H.Ø., Lauknes, T.R., Larsen, Y., Corner, G.D., Bergh, S.G., Dehls, J.F. and Kierulf, H.P., 2017. Visualizing and interpreting surface displacement patterns on unstable slopes using multi-geometry satellite SAR Interferometry (2D InSAR). Remote Sensing of Environment, 191: 297-312.http://dx.doi.org/10.1016/j.rse.2016.12.024

Etzelmueller, B., Ødegard, R.S., Berthling, I. and Sollid, J.L., 2001. Terrain parameters and remote sensing data in the analysis of permafrost distribution and periglacial processes: examples from southern Norway. Permafrost and Periglacial Processes, 12: 79-92.

Etzelmüller, B., 2013. Recent advances in mountain permafrost research. Permafrost and Periglacial Processes, 24(2).doi: 10.1002/ppp.1772

Gisnås, K., Etzelmüller, B., Lussana, C., Hjort, J., Sannel, A.B.K., Isaksen, K., Westermann, S., Kuhry, P., Christiansen, H.H., Frampton, A. and Åkerman, H.J., 2016. Permaforst map of Norway, Sweden and Finland. Permafrost and Periglacial Processes: 359-378.doi: 10.1002/ppp.1922

Haeberli, W., 2013. Mountain permafrost - research frontiers and a special long-term challenge. Cold Regions Science and Technology, 96: 71-76.http://dx.doi.org/10.1016/j.coldregions.2013.02.004

Harris, C., Arenson, L.U., Christiansen, H.H., Etzelmüller, B., Frauenfelder, R., Gruber, S., Haeberli, W., Hauck, C., Hoelzle, M., Humlum, O., Isaksen, K., Kääb, A., Kern-Luetschg, M.A., Lehning, M., Matsuoka, N., Murton, J.B., Noetzli, J., Phillips, M., Ross, N., Sepp‰l‰, M., Springman, S.M. and Vonder Muehll, D., 2009. Permafrost and climate in Europe: Monitoring and modelling thermal, geomorphological and geotechnical responses. Earth-Science Reviews, 92(3-4): 117-171

Harris, C., Kern-Luetschg, M., Smith, F. and Isaksen, K., 2008. Solifluction processes in an area of seasonal ground freezing, Dovrefjell, Norway. Permafrost and Periglacial Processes, 19: 31-47.doi: 10.1002/ppp.609

Hjort, J. and Luoto, M., 2013. Statistical methods for geomorphic distribution modeling. In: J.F.E.-i.-c. Shroder and A.C.W.V.e. Baas (Editors), Treatise on

Geomorphology. Quantitative modeling of Geomorphology. Academic Press, San Diego, pp. 59-73.

Hjort, J., Ujanen, J., Parviainen, M., Tolgensbakk, J. and Etzelmüller, B., 2014. Transferability of geomorphological distribution models: Evaluation using solifluction features in subarctic and Arctic regions. Geomorphology, 204(0): 165-176.http://dx.doi.org/10.1016/j.geomorph.2013.08.002

Kääb, A., Huggel, C., Fischer, L., Guex, S., Paul, F., Roer, I., Salzmann, N., Schlaefli, S., Schmutz, K., Schneider, D., Strozzi, T. and Weidmann, Y., 2005. Remote sensing of glacier- and permafrost-related hazards in high mountains: an overview. Nat. Hazards Earth Syst. Sci., 5: 527-554

Kenyi, L. and Kaufmann, V., 2003. Estimation of rock glacier surface deformation using SAR interferometry data. IEEE Transactions on Geoscience and Remote Sensing, 41: 1512-1515.doi: :10.1109/TGRS.2003.811996

Kverndal, A.-I. and Sollid, J.L., 1993. Late Weichselian glaciation and deglaciation in northeastern Troms, northern Norway. Norsk Geografisk Tidsskrift - Norwegian Journal of Geography, 47(3): 163-177.doi:10.1080/00291959308621975

Larsen, Y., Engen, G., Lauknes, T.R., Malnes, E. and Høgda, K.A., 2005. A generic differential interferometric SAR processing system, with applications to land subsidence and snow-water equivalent retrieval. In: E. ESRIN (Editor), Fringe ATSR Workshop 2005, Frascati, Italy, pp. 6.

Lauknes, T.R., Piyush Shanker, A., Dehls, J.F., Zebker, H.A., Henderson, I.H.C. and Larsen, Y., 2010. Detailed rockslide mapping in northern Norway with small baseline and persistent scatterer interferometric SAR time series methods. Remote Sensing of Environment, 114(9): 2097-2109.10.1016/j.rse.2010.04.015

Liu, L., Schaefer, K., Zhang, T. and Wahr, J., 2012. Estimating 1992-2000 average active layer thickness on the Alaskan North Slope from remotely sensed surface subsidence. J. Geophys. Res., 117(F1): F01005.doi: 10.1029/2011jf002041

Liu, L., Zhang, T. and Wahr, J., 2010. InSAR measurements of surface deformation over permafrost on the North Slope of Alaska. J. Geophys. Res., 115(F3): F03023.10.1029/2009jf001547

Matsuoka, N., 2001. Solifluction rates, processes and landforms: a global review. Earth-Science Reviews, 55(1-2): 107-134

MET, 2017. eklima. Free access to weather- and climate data from Norwegian Meteorological Institute form historical data to real time observations. http://www.eklima.no.

Price, E.J. and Sandwell, D.T., 1998. Small-scale deformations associated with teh 1992 Landers, California, earthquake mapped by synthetic aperture radar interferometry phase gradients. Journal of Geophysical Research, 103.doi: 10.1029/98JB01821

Short, N., Brisco, B., Coutore, N., Pollard, W., Murnaghan, K. and Budkewitsch, P., 2011. A comparison of TerraSAR-X, RADARSAT-2 and ALOS-PALSAR interferometry for monitoring permafrost environments, case study from Herschel Island, Canada. Remote Sensing of Environment, 115: 3491-3506.doi: 10.1016/j.rse.2011.08.012

Shur, Y., Hinkel, K.M. and Nelson, F.E., 2005. The transient layer: implications for geocryology and climate-change science. Permafrost and Periglacial Processes, 16(1): 5-17.http://dx.doi.org/10.1002/ppp.518

Strozzi, T., Kääb, A. and Frauenfelder, R., 2004. Detecting and quantifying mountain permafrost creep from in situ inventory, space-borne radar interferometry and airborne digital photogrammetry. Int. J. Remote Sensing, 25(15): 2919-2931

Tolgensbakk, J. and Sollid, J.L., 1988. Kåfjord, kvartærgeologi og geomorfologi 1:10 000, Geografisk Institutt, University of Oslo.